Proceedings of ISERME 2025
19-20 September 2025
https://doi.org/10.31705/ISERME.2025.1

Evaluation of Image-Based Segmentation Algorithms for Discontinuity Detection

Najeeba MNF, Silva KDC, De Silva KPK, Xavier SA, Dassanayake ABN and *Thiruchittampalam S

Department of Earth Resources Engineering, University of Moratuwa, Sri Lanka

*Corresponding author – surekat@uom.lk

Abstract

Accurate detection of discontinuities is critical to determine rock mass features such as block geometry, joint orientation, and potential failure surfaces, which govern structural stability in mining and geotechnical applications. Manual methods of detecting discontinuities are often time-consuming, expose personnel to hazardous situations, and are susceptible to biased judgement. In response, image processing techniques like image segmentation have been increasingly adapted to detect discontinuities from rock outcrop images. This study evaluates the performance of traditional and machine learning segmentation methods to identify a higher accuracy workflow for discontinuity detection and the following methodology was employed: RGB rock outcrop images were manually annotated to establish ground truth masks, pre-processed with noise-reduction filters and then processed using traditional Gradient-based operators, Canny edge detection, thresholding and machine learning approaches, U-net, Holistically-Nested Edge Detection (HED), and Segment Anything Model (SAM). The performance of these methods was quantified by evaluating the Boundary F1 score against the ground truth masks. Among discontinuity-based traditional segmentation methods, on a scale of 0 to 1, Canny edge detection with morphological gradient achieved F1 scores of 0.194 and 0.196, while among similarity-based segmentation methods, dilation of eroded threshold images achieved F1 scores of 0.264 and 0.202. For machine learning methods, SAM outperformed the other methods by achieving F1 scores of 0.752 and 0.632, but caused over-segmentation in highly discontinuous regions. The findings highlight the significance of combining computationally efficient traditional methods with targeted preprocessing for low-resource settings and underscore the trade-off between machine learning accuracy and its infrastructural demands.

Keywords – Rock mass characterization, Traditional segmentation, Machine learning based segmentation, Boundary F1 score

1 Introduction

Discontinuities like bedding planes, joints, foliation, and faults impact the mechanical strength, permeability, and deformational behaviour of a rock mass, directly affecting its stability [1]. Current methods to detect discontinuities rely on manual practices performed by field geologists and engineers, utilizing tape measures, callipers, or scale references, and by conducting scanline surveys or window mapping [2]. However, manual methods are limited by observer bias, physical accessibility and are often time-consuming and expose personnel to hazardous environments [3].

Advancements in imaging sensors and image processing techniques have been applied to overcome the limitations of manual methods when detecting rock discontinuities. Image segmentation, a technique of image processing, is the process of partitioning an image into

multiple segments, where each segment represents a different object in the image. These methods have been used to distinguish features of interest, such as cracks, joints, and edges, from the surrounding rock surface by partitioning the image based on changes in pixel intensity. Traditional image segmentation methods such as Sobel, Roberts, and Prewitt operators were utilized to map discontinuities on walls of an iron ore mine, which are simple and fast processing but yield results that are highly sensitive to noise [4]. Canny, the most common Gaussian-based operator is relatively more robust for noisy images and provides thinner edges, but it also results in blurred edges, fake or missed edges due to manual parameter selection and detection of pulse-like edges as double trace lines [5]. In threshold segmentation, manual selection of thresholds is difficult to achieve due to the interference of noises and low contrast, and Otsu's segmentation is sensitive to noise and requires clear bimodal distribution of the pixel intensity values to effectively obtain the threshold value automatically [6]. The K-way normalized cuts algorithm, a graph-based method, allows extraction by partitioning an image into multiple segments without any bias, but it can also lead to over-segmentation [7]. Overall, traditional segmentation algorithms, while helpful for identifying edges, face significant limitations such as sensitivity to lightning changes and noise, indistinct boundaries [8], and manual parameter selection, while single segmentation methods often result in either under-segmentation or over-segmentation of rock discontinuities [9].

To address the drawbacks of traditional approaches, machine learning segmentation methods have been utilized to automate and improve rock discontinuity detection. Artificial Neural Network (ANN) was employed as a classification method in a study focusing on segmentation of rock grains in bulk material to determine the borders of rock grains, but it required large amounts of labelled data and took a long time to train, which can be less ideal for smaller projects [10]. Convolutional Neural Network (CNN) was used in a study focusing on presenting a classification framework to classify rock blocks in slopes, achieving 95% accuracy and 93% precision by learning detailed patterns, but it required lots of labelled images and higher computational power [11]. Mask R-CNN was employed to segment rock particles, reaching 92.3% average precision [12], and the same method was used to segment tunnel rock fragments, achieving 90.2% mean average precision, on a workstation with an i9-9900 K CPU and a 2080Ti GPU, requiring higher computational power and large datasets [13]. U-net was used to process images to detect weak zones in the ground, but the model struggled with images with high intensity of noise, making it difficult to segment complex rock mass images [14]. Tunnel performance was studied by using experimental tests, and Segment Anything Model (SAM) aided by analyzing images to identify materials like shotcrete or steel arches, making it easier to compare real and simulated conditions, but it struggled with very small or overlapping objects, which can affect its accuracy in detailed tunnel images [15]. In summary, machine-learning methods require large amounts of labelled data, high computer power and takes a long time to train.

As such, recent studies have highlighted problems when using image segmentation algorithms to detect rock discontinuities. These unresolved trade-offs between accuracy, robustness, and operational feasibility, necessitate a systematic evaluation of segmentation workflows. To address these concerns, this study focuses on evaluating traditional and machine-learning based segmentation algorithms, combined with preprocessing techniques, to provide a methodological framework to implement basic discontinuity detection in a resource constrained environment.

2 Methodology

2.1 Methodology Overview

The study employs a structured workflow to comparatively evaluate traditional segmentation, including gradient-based operators (Sobel, Roberts, Prewitt, Scharr, Farid), Canny edge detection, and thresholding techniques, alongside machine learning approaches, U-Net, Holistically-Nested Edge Detection (HED), and SAM (Figure 1).

2.2 Data Collection and Preparation

The study utilized two RGB rock outcrop images of 875×875 pixels sourced from a public GitHub repository https://github.com/rahulprabhakaran/Automatic-Fracture-Detection-Code/tree/master/Examples/Bingie_Bingie, labelled as Study Area 1 (SA1) and Study Area 2 (SA2) for easy identification throughout the

course of the study. The ImageJ software was utilized to manually annotate the two rock outcrop images to establish a ground truth for the evaluation of the selected segmentation methods (Figure 2).

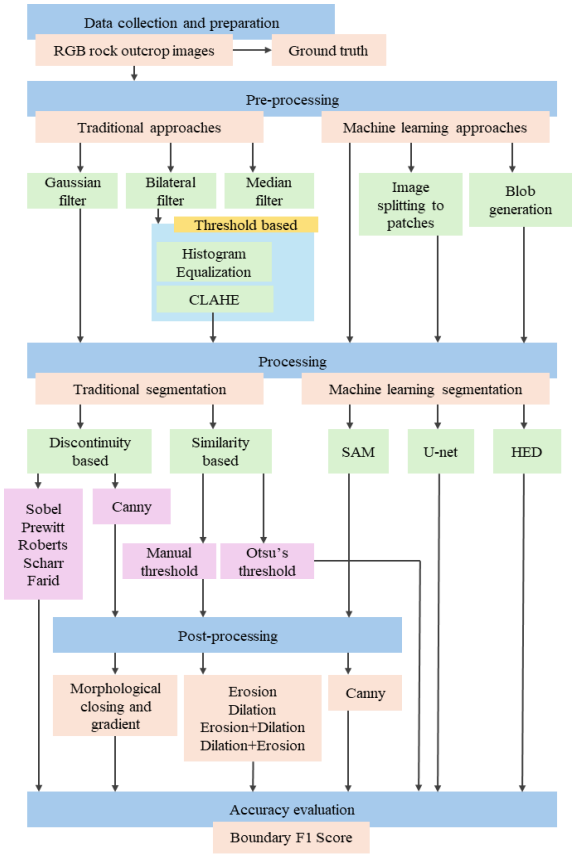

Figure 1: Workflow of the research methodology

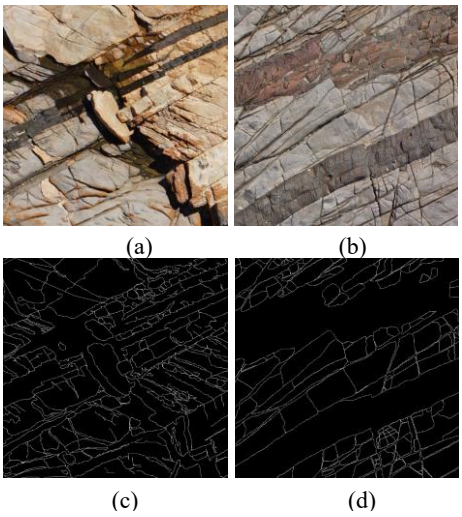

Figure 2: (a) Study Area 1 (b) Study Area 2 (c) Ground truth of Study Area 1 (d) Ground truth of Study Area 2

2.3 Application of Segmentation Methods

2.3.1 Traditional Segmentation Methods

Initially, preprocessing steps were implemented by applying Gaussian, median and bilateral filters to remove noise from the images. Among the preprocessing filters, the median and Gaussian filters resulted in images with a high blur intensity leading to the blurring of rock block boundaries, while the bilateral filter retained the sharpness of the rock boundaries and achieved noise suppression. Due to this reason, images pre-processed using the bilateral filter were used for further processing. For thresholding, the images were further pre-processed by applying histogram equalization and contrast limited adaptive histogram equalization (CLAHE) to improve contrast in low-light regions and to make the foreground and background intensities more distinct for the ease of manual threshold selection.

The pre-processed images were evaluated with Sobel, Prewitt, Roberts, Scharr, and Farid gradient edge-based segmentation operators. The Canny edge detector was evaluated with varying thresholds and further post-processed using morphological closing, opening, and gradient operations with a (3,3) kernel size. Manual thresholding and automated global thresholding using Otsu's algorithm were performed on the images pre-processed using histogram equalization and CLAHE. Afterwards, iterative erosion and dilation with (3,3) kernel size were applied to the thresholded images, to clean further noise and refine the obtained segmentation.

2.3.2 Machine Learning Segmentation Methods

Three machine learning approaches were implemented to the rock outcrop images: U Net, HED, and SAM.

To apply U-Net for segmentation of discontinuities, the two rock outcrop images and their corresponding manually annotated masks were split into 36 overlapping patches of size 350×350 pixels using a sliding window approach with an overlap of 100 pixels (Figure 3). The U-Net model was trained and validated using the patched images of SA2, and the model was tested on the patched images of SA1.

Figure 3: Sample patches of Study Area 2 and their corresponding ground truth

The training process included a loss function with binary cross-entropy with logits to handle class imbalance between rock discontinuities and the background, an optimizer of stochastic gradient descent (SGD) with a momentum of 0.9 and a learning rate of 0.001, 50 epochs with early stopping monitored on validation loss. The training leveraged CUDA acceleration on a GPU, and the inference was tested on CPU/GPU. The trained model was then utilized to predict masks for 350×350 testing dataset patches which were resized to 256×256 before inference.

The HED framework was implemented using a pre-trained Caffe model with OpenCV's deep neural network module. The images were pre-processed by converting them into blobs with the key parameters being a scaling factor of 1.2, standard mean of [104.0,116.7,122.7], and spatial resolution of the original image dimensions to minimize resolution loss. The generated blob was passed through the HED network to generate a grayscale edge map.

SAM was employed for segmentation with a vision transformer-huge (ViT-H) backbone. SAM automatic mask generator was utilized to generate a total of 216 masks with 32 points per side that are to be distributed uniformly across the image to seed potential regions, an IoU threshold of 0.8 to filter low-confidence predictions, a stability score of 0.94 to retain masks with consistent segmentation across augmentations, minimum mask area of 100 pixels to discard fragmented artifacts, and 1 hierarchical crop layer with a downscale factor of 2 to handle large-scale geological features.

Canny was then applied to each of the 216 masks generated to extract object boundaries and generate one binary mask. The detected edges were then combined into a unified edge map using bitwise OR operations.

2.4 Evaluation Framework

To quantify the accuracy of the predicted boundaries through segmentation methods against the ground truth, the Boundary F1 score metric was implemented. The basic components of this metric are precision and recall. Precision represents the percentage of predicted boundary pixels that match a ground truth boundary. Recall represents the percentage of ground truth boundary pixels that are matched by predicted boundaries. Boundary F1 score has been used as an evaluation metric in a study on comparing the segmentation effectiveness of multiple deep learning approaches on various types of complex fluorescence nuclear images [16].

Initially, the ground truth and predicted masks were binarized to 0s and 1s. Both masks were then thinned to 1-pixel wide boundaries to eliminate thickness discrepancies. A distance threshold of 10 pixels was defined to account for minor misalignments in edge localization and a kernel was applied to dilate the skeletonized ground truth to create a buffer zone around true edge. A continuity penalty was applied to account for the disconnected edge fragments in the predicted mask.

$$\mathbf{F1} = \frac{\mathbf{2 * Adjusted\ Precision * Recall}}{\mathbf{Adjusted\ Precision + Recall}} \quad (1)$$

Where, adjusted precision is the fraction of predicted edges within the dilated ground truth buffer with the continuity penalty and recall is the fraction of ground truth edges within the dilated predicted buffer.

2.5 Implementation Environment

All algorithms were developed in Python 3.8 using the Spyder IDE from anaconda distribution. Key libraries include OpenCV for image processing, scikit-image for morphological operations, NumPy for numerical operations, TensorFlow and PyTorch for machine learning model implementations, Patchify for dividing images into training patches, and Matplotlib for generating qualitative comparisons and visualization. Computational experiments were conducted on a workstation with an Intel i7 CPU (16GB RAM) and an NVIDIA RTX 3060 GPU, with CUDA

acceleration for machine learning model training and inference

3 Results and Discussion

3.1 Traditional Segmentation

The comparative evaluation of traditional segmentation methods on SA1 and SA2 demonstrated distinct segmentation characteristics across different preprocessing, edge detecting, thresholding, and post-processing workflows.

The study area images pre-processed using bilateral filter were then processed using edge filters, which resulted in images with a higher degree of noise and over-segmentation. Although images processed by Roberts, Sobel, Scharr, Prewitt, and Farid resulted in relatively high F1 scores, visually, the results were over-segmented with multiple detections for single boundaries. Due to many edges being in close proximity and detection of false edges, misleading boundary F1 scores were obtained (Figure 4).

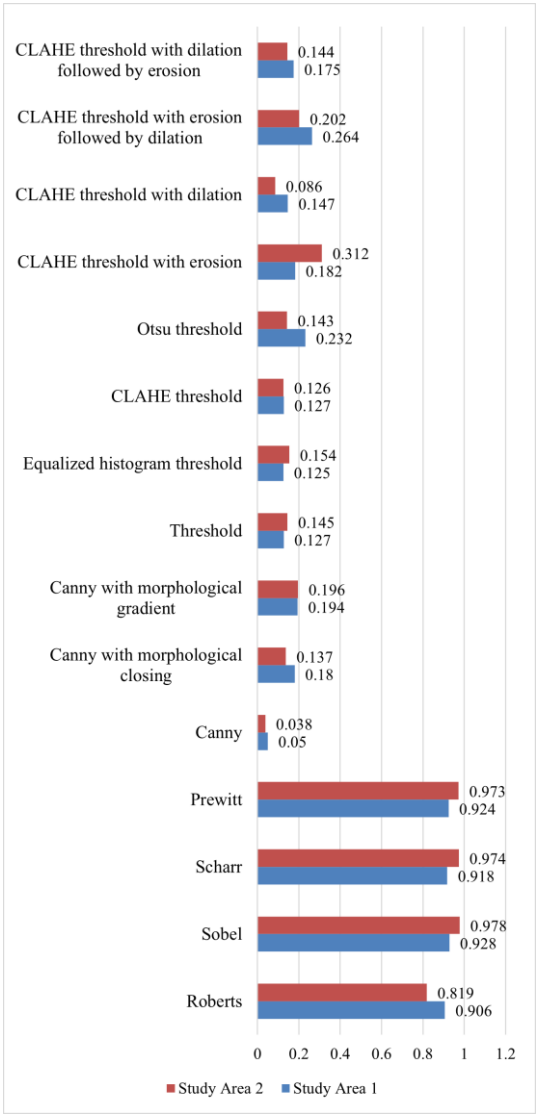

Figure 4: Boundary F1 scores for traditional segmentation methods

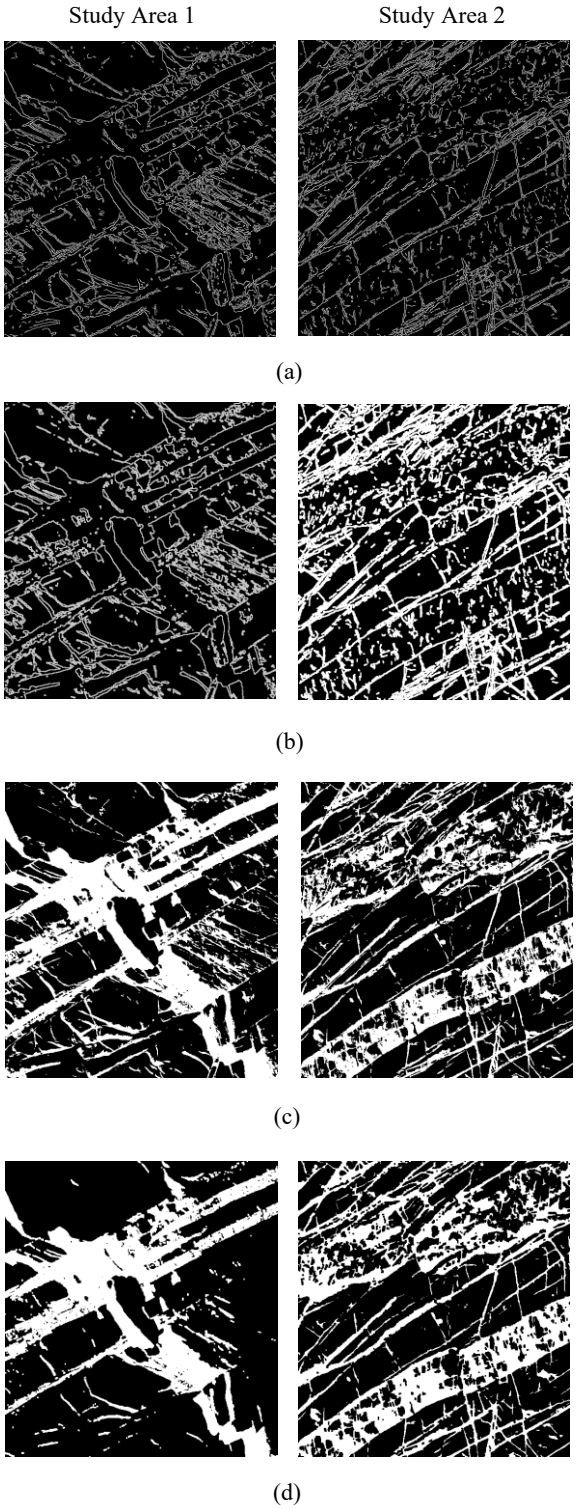

Figure 5: (a) Canny (b) Canny with morphological gradient (c) Thresholding with CLAHE (d) CLAHE threshold with erosion followed by dilation

Among the discontinuity-based methods applied to the images pre-processed using bilateral filter, the Canny algorithm outperformed by leveraging Gaussian smoothing and hysteresis thresholding, achieving F1 scores of 0.05 and 0.038 for SA1 and SA2 respectively, producing sharper edges with reduced sensitivity to noise and better visualization of discontinuities than that of edge filters (Figure 5).

However, it also resulted in fragmented boundaries, unclear segmentation in complex rock mass regions, and the persistence of double-trace lines in narrow apertures. Post-processing with morphological closing operations enhanced performance by reducing white specks in the image and smoothing edges, but at the cost of closing small gaps between adjacent blocks. Morphological gradient further improved the segmentation with relatively better connectivity of edges, though thicker boundaries obscured fine cracks occasionally (Figure 5). Canny requires subjectivity when assigning a threshold value, and morphological operations distort edge geometry, limiting their usage for complex rock masses.

Among the similarity-based methods, Threshold segmentation achieved F1 score values of 0.127 and 0.145 for SA1 and SA2 respectively, resulting in sharp edges between light and dark areas with better visualization of discontinuities than those achieved by discontinuity-based algorithms. However, edges remained discontinuous. For SA1, Otsu's threshold achieved the highest F1 score of 0.232 due to its automatic global threshold selection, while for SA1, segmenting with an equalized histogram achieved the highest F1 score of 0.154. Otsu's reliance on bimodal distribution led to the drop in F1 score for SA2 for areas where overlapping blocks create unimodal distribution, and the resulting images were highly affected by noise compared to manual thresholding. Despite resulting in over enhancing of noise in highly textured regions, since thresholding with CLAHE visually resulted in better segmenting while preserving finer details and reducing noise in other areas, morphological processing was applied to images thresholded with CLAHE (Figure 5).

Application of morphological operations shows better results with thresholded images than with Canny segmented images. Both SA1 and SA2 achieve higher F1 scores than that of images segmented only with threshold, resulting in thick edges with better connectivity. While dilation reduces the presence of noise, it also leads to the loss of detected boundaries in shadowed regions. Application of dilation to eroded images resulted in reduced noise and better edge connectivity, while application of erosion to dilated images resulted in the joining of broken edges and filling of small cracks but also smoothened out some necessary details (Figure 5).

3.2 Machine Learning Segmentation

Among the machine learning methods, U-Net resulted in the least F1 score, while the other two methods achieved considerably higher F1 scores than that of the traditional segmentation results. Predicted boundaries of SA2 using U-Net with images of SA1 as the training dataset resulted in a F1 score of 0.268 (Figure 7). Although, the resulting images were primarily focused on the segmentation of shadows or darker coloured regions in the testing images (Figure 6).

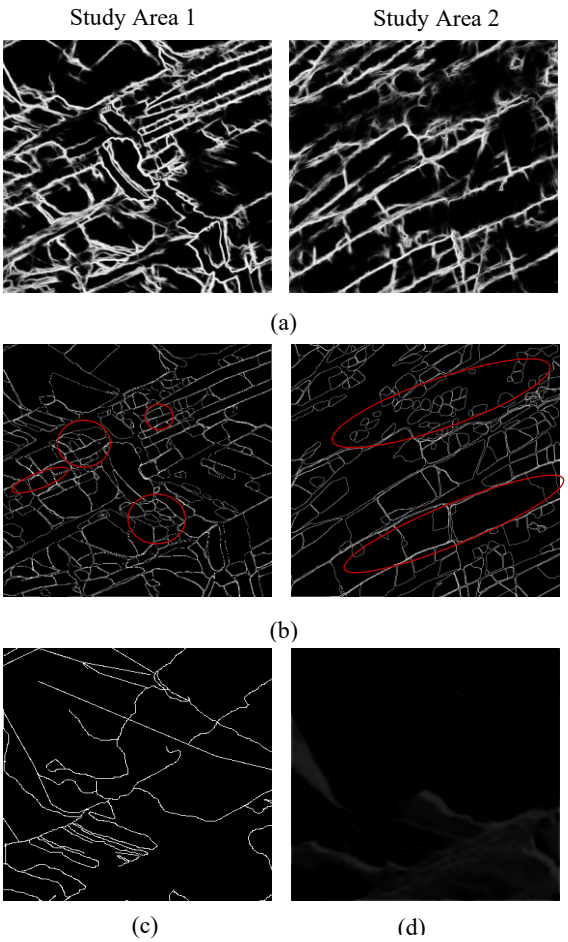

Figure 6: (a) HED (b) SAM (c) Ground truth of a patch of Study Area 1 (d) U-Net prediction of the same patch of Study Area 1

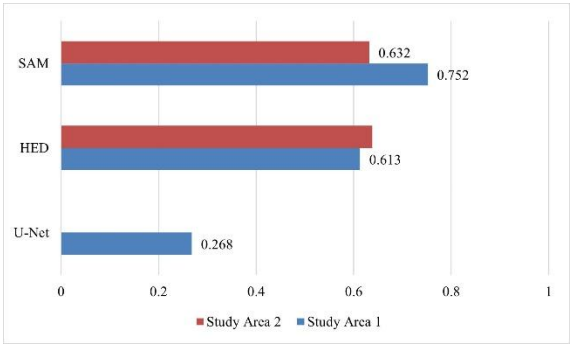

Figure 7: Boundary F1 Scores of machine learning methods

HED proves to be successful in segmenting discontinuities delineating large blocks, but results in blurred edges and the loss of smaller edges. While HED results lack distinct boundaries defined by precise lines, the resulting images have less noise than those of traditional segmented images and have better visualization of the discontinuities than that achieved by traditional segmentation (Figure 6).

SAM resulted in clear segmentation of discontinuities of both large and smaller rock blocks. However, it results in over-segmentation in highly discontinuous areas where separate rock blocks cannot be visually identified (Figure 6).

4 Conclusion

Effective detection of rock discontinuities is essential for stability assessment of rock mass, and existing segmentation methods require careful trade-offs between score, processing time, and available resources. A comparison between the cluster of segmentation approaches reveals inherent limitations that dictate their practical utility. For rapid surveys with minimal hardware, bilateral filtering followed by Canny edge detection and a morphological gradient operation offers a practical solution, yet one that depends on manual threshold adjustment. In a similar environment, for scenarios involving images with more distinct bimodal distribution between pixel intensities of the foreground and background, thresholding enhanced by CLAHE combined with iterative morphological refinements offers a well-balanced alternative. In contrast, when higher boundary definition is required and adequate GPU resources are available, SAM achieves superior segmentation but requires post-processing to control the tendency of over-segmentation in complex textured areas. Key limitations of this study include dataset constraints, manual parameter tuning, lack of adequate computational resources, potential annotation subjectivity and unresolved over-segmentation in complex terrains. For future direction, studies should focus on hybrid frameworks by integrating traditional pre-processing with lightweight machine learning, optimization of parameters automatically, incorporation of 3D spatial data to enhance contextual awareness, and utilizing more efficient accuracy evaluation metrics. Such advancements would bridge the gap between theoretical performance and real-world application viability, advancing the detection of discontinuities.

Acknowledgments

The authors wish to extend their gratitude to all academic and non-academic staff members of the Department of Earth Resources Engineering, University of Moratuwa for their assistance throughout the course of this study.

References

[1] H. Daghigh, D. D. Tannant, V. Daghigh, D. D. Lichti, and R. Lindenbergh, “A critical review of discontinuity plane extraction from 3D point cloud data of rock mass surfaces,” *Comput. Geosci.*, vol. 169, p. 105241, Dec. 2022, doi: 10.1016/j.cageo.2022.105241.

[2] R. Yarahmadi, R. Bagherpour, L. M. O. Sousa, and S.-G. Taherian, “How to determine the appropriate methods to identify the geometry of in situ rock blocks in dimension stones,” *Environ. Earth Sci.*, vol. 74, no. 9, pp. 6779–6790, Nov. 2015, doi: 10.1007/s12665-015-4672-4.

[3] M. Azarafza, E. Asghari-Kaljahi, and H. Akgün, “Assessment of discontinuous rock slope stability with block theory and numerical modeling: a case study for the South Pars Gas Complex, Assalouyeh, Iran,” *Environ. Earth Sci.*, vol. 76, no. 11, p. 397, Jun. 2017, doi: 10.1007/s12665-017-6711-9.

[4] M. Mohebbi, A. Yarahmadi Bafghi, M. Fatehi Marji, and J. Gholamnejad, “Rock mass structural data analysis using image processing techniques (Case study: Choghart iron ore mine northern slopes),” *J. Min. Environ.*, no. Online First, May 2016, doi: 10.22044/jme.2016.629.

[5] M. Huang, Y. Liu, and Y. Yang, "Edge detection of ore and rock on the surface of explosion pile based on improved Canny operator," *Alex. Eng. J.*, vol. 61, no. 12, pp. 10769–10777, Dec. 2022, doi: 10.1016/j.aej.2022.04.019.

[6] Y. Tang, L. He, W. Lu, X. Huang, H. Wei, and H. Xiao, "A novel approach for fracture skeleton extraction from rock surface images," *Int. J. Rock Mech. Min. Sci.*, vol. 142, p. 104732, Jun. 2021, doi: 10.1016/j.ijrmms.2021.104732.

[7] J. Zhu, Y. Xia, B. Wang, Z. Yang, and K. Yang, "Research on the Identification of Rock Mass Structural Planes and Extraction of Dominant Orientations Based on 3D Point Cloud," *Appl. Sci.*, vol. 14, no. 21, Art. no. 21, Jan. 2024, doi: 10.3390/app14219985.

[8] B. Wang and Z. Yang, "Edge detection algorithm based on valley lines and watershed," *J. Phys. Conf. Ser.*, vol. 2010, no. 1, p. 012034, Sep. 2021, doi: 10.1088/1742-6596/2010/1/012034.

[9] F. Bai, M. Fan, H. Yang, and L. Dong, "Image segmentation method for coal particle size distribution analysis," *Particuology*, vol. 56, pp. 163–170, Jun. 2021, doi: 10.1016/j.partic.2020.10.002.

[10] K. Nurzynska and S. Iwaszenko, "Application of texture features and machine learning methods to grains segmentation in rock material images," *Image Anal. Stereol.*, Jun. 2020, doi: 10.5566/ias.2186.

[11] H. Zhu, M. Azarafza, and H. Akgün, "Deep learning-based key-block classification framework for discontinuous rock slopes," *J. Rock Mech. Geotech. Eng.*, vol. 14, no. 4, pp. 1131–1139, Aug. 2022, doi: 10.1016/j.jrmge.2022.06.007.

[12] F. Ogunkeye, L. Shan, and X. Hei, "Rock Particle Segmentation Using Mask R-CNN," Apr. 09, 2024, *Environmental and Earth Sciences*. doi: 10.20944/preprints202404.0624.v1.

[13] W. Qiao *et al.*, "Deep learning-based pixel-level rock fragment recognition during tunnel excavation using instance segmentation model," *Tunn. Undergr. Space Technol.*, vol. 115, p. 104072, Sep. 2021, doi: 10.1016/j.tust.2021.104072.

[14] M. V. Ronkin, E. N. Akimova, and V. E. Misilov, "Review of deep learning approaches in solving rock fragmentation problems," *AIMS Math.*, vol. 8, no. 10, pp. 23900–23940, 2023, doi: 10.3934/math.20231219.

[15] L. Zhang, T. Sherizadeh, Y. Zhang, M. Sunkpal, H. Liu, and Q. Yu, "Stability analysis of three-dimensional rock blocks based on general block method," *Comput. Geotech.*, vol. 124, p. 103621, Aug. 2020, doi: 10.1016/j.compgeo.2020.103621.

[16] F. Kromp *et al.*, "Evaluation of Deep Learning Architectures for Complex Immunofluorescence Nuclear Image Segmentation," *IEEE Trans. Med. Imaging*, vol. 40, no. 7, pp. 1934–1949, Jul. 2021, doi: 10.1109/TMI.2021.3069558

.